Journal of Testing and Evaluation

doi:10.1520/JTE20160439 / Vol. 46 / No. 2 / March 2018 / available online at www.astm.org

C. Demian,[1] D. Ferreño,[2] E. Ruiz,[1] and J. A. Casado[1]

Study of the Efficiency and Temperature Loss Caused by Degassing and Filtration of $AlSi_9Cu_3$ Alloy

Reference

Demian, C., Ferreño, D., Ruiz, E., and Casado, J. A., "Study of the Efficiency and Temperature Loss Caused by Degassing and Filtration of $AlSi_9Cu_3$ Alloy," *Journal of Testing and Evaluation*, Vol. 46, No. 2, 2018, pp. 772–782, https://doi.org/10.1520/JTE20160439. ISSN 0090-3973

ABSTRACT

This paper presents a research on the ability of the techniques of degassing and filtration to improve the properties of the $AlSi_9Cu_3$ alloy. The study includes four types of samples: (1) non-treated, (2) filtered, (3) degassed, and (4) filtered and subsequently degassed samples. Degassing was carried out using nitrogen gas, whereas a 20-pores-per-inch (ppi) alumina filter was used for filtering the samples. The analysis was focused on three aspects: First, the influence of these processes on the porosity was determined by means of software to analyze micrographs. Second, the distribution of phases and the presence of inclusions were obtained by combining optical and scanning electron microscopy. Finally, the temperature loss as a result of each of the treatments received by the material was measured. This information is particularly relevant in view of the subsequent use of the molten material to manufacture parts through high-pressure die casting.

Keywords

degassing, filtration, $AlSi_9Cu_3$ alloy, porosity, loss of temperature, microstructure

Manuscript received August 25, 2016; accepted for publication December 19, 2016; published online November 10, 2017.

[1] LADICIM (Laboratory of Materials Science and Engineering), Univ. of Cantabria, E.T.S. de Ingenieros de Caminos, Canales y Puertos, Av/Los Castros 44, 39005 Santander, Spain

[2] LADICIM (Laboratory of Materials Science and Engineering), Univ. of Cantabria, E.T.S. de Ingenieros de Caminos, Canales y Puertos, Av/Los Castros 44, 39005 Santander, Spain (Corresponding author), e-mail: ferrenod@unican.es

Introduction and Objectives of this Research

The production and consumption of aluminum alloys worldwide has grown steadily in the last few decades because of the interesting properties of this material. In particular, its low density, good mechanical properties, and corrosion resistance make it an ideal material for many industrial applications. For instance, density is particularly appreciated in the transportation industry because it permits lighter vehicles to be manufactured and, consequently, a reduction in fuel consumption and CO_2 emissions [1].

Most of the aluminum alloy parts are manufactured through the high-pressure die-casting method (HPDC). Usually, they present pores in their mass that reduce the final quality of the product and may even lead to its rejection by the end client. Moreover, the presence of inclusions of various origins can determine the acceptability of the final component [2,3].

Regarding porosity, hydrogen is the only gas that is appreciably soluble in aluminum and its alloys. Hydrogen forms whenever molten aluminum comes into contact with water vapor. Typical gas porosities result from hydrogen contained in the liquid aluminum according to, among others, the following chemical reaction: $2Al + 3H_2O \rightarrow Al_2O_3 + 6H$ or/and from decomposition of hydrocarbons (coatings, lubricants). The solubility of hydrogen in aluminum decreases drastically during solidification [3,4]; therefore, gas tends to form bubbles when the melt solidifies, leading to the presence of porosity in the final parts. Two types of forms of hydrogen porosity may occur in cast aluminum. Of greater importance is interdendritic porosity, which is encountered when hydrogen contents are sufficiently high; secondary or micro-size porosity occurs when dissolved hydrogen contents are low. It is often assumed that secondary porosity may not always be undesirable [3]. The detrimental effects arising from the presence of an excess of dissolved hydrogen in aluminum have been reported in the literature, paying particular attention to the influence of mechanical properties [3–9]. Regardless of the origin and nature of porosity, material discontinuities may cause a reduction in the cross section; in addition, they can be a site of initiation of cracking and its further propagation, resulting in irreversible degradation of the casting product during exploitation [10].

With regard to the presence of inclusions, aluminum and its alloys readily oxidize in both the solid and molten states to provide a continuous self-limiting film. The rate of oxidation increases with temperature and is substantially greater in molten than in solid aluminum. The entrainment of oxide particles in the molten aluminum resists gravity separation because their density is similar to that of the liquid. In addition to oxides, a number of compounds such as carbides or borides can be considered inclusions in cast structures. Under all conditions, inclusions are damaging for the mechanical properties. The gross effect of inclusions is to reduce the effective cross section of the part being loaded. The more devastating effect on properties is that of stress concentration when inclusions appear at or near the surface of parts or specimens. Because of this same reason, fatigue performance is reduced under the later condition by the notch effect [3,4].

To optimize the final quality of aluminum components, the industry has developed various techniques for cleaning and treating the material in the molten state. At present, there are a large number of methods available such as filtration, sedimentation, agglomeration, ultrasonic degassing, vacuum degassing, inert gas degassing, among others. This paper analyses two of these methods, namely, degassing by means of an inert gas and filtration.

Degassing is a technique used to reduce the amount of gas inclusions present in the molten material in the form of bubbles [11,12]. The method of degassing consists of bubbling an inert gas (usually nitrogen or argon) through a graphite rotor that spins inside the liquid alloy dispersing very small gas bubbles. The degassing process is based upon the capacity of these tiny bubbles to absorb the hydrogen dissolved into the metallic bath leading to the formation of hydrogen molecules. Then, the inert gas bubbles migrate to the surface of the metallic bath where they can be easily removed [13] or eliminated in the atmosphere. Moreover, degassing is capable of eliminating nonmetallic inclusions as a result of the collision with the gas bubbles that facilitates the flotation of these impurities. In this sense, Dispinar and others [13–15] conducted a study with aluminum alloy A356 where they showed that, after degassing, a layer of dross is formed on the surface of the liquid alloy, which contains a significant amount of non-metallic inclusions. Finally [15], because of the agitation caused by the gas passing through the molten material, an improved thermal and chemical homogenization of the liquid bath is achieved.

The process of filtration has the main objective of removing non-metallic inclusions [16–18]. Ceramic foam filters (CFFs) consist of a labyrinth-type structured ceramic material in which a very effective cleaning of the aluminum melt happens by deep bed filtration effects. Filter plates are commercially available in different sizes, thicknesses (normally 50 mm), and pore sizes between 10 ppi to 80 ppi (pores per inch). Ceramic foam filters were first used to filter aluminum alloys but, over the years, they were employed in a large variety of metals, including cast iron [19]. Filters are fabricated with several refractory materials such as Al_2O_3, ZrO_2, or mullite [20]. Filtration efficiency is influenced, among others, by the nature of the molten material, the number, size and distribution of inclusions, and the flow velocity of the alloy through the filter [21].

The fabrication of the samples analyzed in this research has been carried out in an industrial facility dedicated to the manufacture of components by means of HPDC. Therefore, in this paper, the actual manufacturing conditions were reproduced making use of real industrial equipment for degassing and filtering. The subsequent analysis of the material was carried out in the facilities of the laboratory LADICIM of the University of Cantabria (Cantabria, Spain).

The $AlSi_9Cu_3$ (A226D) alloy has excellent castability and good mechanical properties [22]. It is used in die-casting and high-pressure die-casting, among others, on the engine component parts, the transmission case, oil pumps, etc. The main objective pursued in this paper is to optimize, through experimental research, the processes of degassing and filtering of the $AlSi_9Cu_3$ (A226D) alloy with respect to two different aspects. On the one hand, the influence of both treatments on the final quality of the material (reduction of porosity and elimination of inclusions) was analyzed. On the other hand, the temperature loss that the molten material undergoes as a result of the application of both treatments, either separately or combined, was determined.

The article is structured as follows: after describing the available material and the experimental methodology, the results obtained are presented and discussed. First, the results corresponding to degassed samples are presented. Then, those results corresponding to filtered and to filtered and degassed samples are

shown. Regarding degassing, the ability of this procedure to eliminate pores as a function of the duration of the treatment was determined; moreover, its influence on the temperature loss of the molten material was measured. In the case of filtering, the main goal was to determine its efficiency to remove inclusions; also, the capacity of filtration, alone and in combination with degassing as a suitable method for reducing the porosity of the material, was studied. Moreover, the loss of temperature in the molten material as a consequence of, first, filtration and then the combination of filtration and degassing, was measured. Finally, a summary thereof and a list of relevant conclusions are provided.

Materials and Methodology

DEGASSING

The material analyzed was melted using a HORMESA reverberatory furnace after which it was poured into a transfer ladle (see **Fig. 1a**) whose capacity of aluminum was ~400 kg. The inner coating of the transfer ladle was made up of refractory concrete with low content of cement and a chemical composition based on corundum and bauxite. The samples were taken directly from the ladle using a small-sized (250 cc) graphite-refractory container. A FOSECO degasser unit (see **Fig. 1b**) acting on the material in the transfer ladle was employed. The inert gas used for degassing was nitrogen with a flow rate of 15 L/min. The samples were treated for 1, 2, or 3 min. The operating sequence is described next: before degassing, one sample of molten material was obtained. Then, after degassing for 1 min, the remaining material in the transfer ladle, another sample was obtained for each non-degassed sample. This process was repeated three times giving rise to three non-degassed (ND) samples (ND_1, ND_2, and ND_3) and their degassed (D) counterparts (D (1)_1, D (1)_2, and D (1)_3); the number "1" between brackets refers to the degassing time. The procedure in the case of degassing during 2 and 3 min was exactly the same. The non-degassed samples ND_4, ND_5, and ND_6 together with the degassed samples D (2)_1, D (2)_2, and D (2)_3 were obtained to determine the influence of degassing for 2 min. Finally, in the case of 3 min, non-degassed samples ND_7, ND_8, and ND_9 together with the degassed samples D (3)_1, D (3)_2, and D (3)_3 were taken. Notice that, according to this sampling method, there is a one-to-one correspondence between non-degassed and degassed samples, which facilitates the subsequent comparison of results. According to this, the total number of non-degassed samples is $3 + 3 + 3 = 9$, corresponding to nine degassed samples (three of them degassed for 1 min, three for 2 min, and the remaining three for 3 min).

The surface temperature of the molten material was determined in the reverberatory furnace and in the transportation ladle (for degassed material, before and after degassing) with a RAYTEC infrared temperature sensor to make it possible to assess the loss of temperature of the process.

After solidifying, each one of the samples was subjected to the following sequence:

- Machining of the sample and extraction of coupons (six coupons were obtained from each sample), see **Fig. 2**.
- Encapsulation of the coupons in resin to be polished.
- Polishing of the coupons to the mirror quality following a suitable protocol for $AlSi_9Cu_3$ alloy.
- Scanning by optical microscopy of the polished surface of the coupons. The microscope used was an Olympus, model BX61.
- Analysis of the micrographs with the Olympus Particle Inspector software to estimate the porosity present in the coupons. This software identifies the pores present on the surface of the coupon and classifies them into categories depending on their size. The program provides a list with the main features of all pores detected including, among others, their size. For the purposes of this research, coupon porosity is defined as the ratio between the total area of the pores and the scanned area of the coupon.

The total number of coupons analyzed was 108 (18 samples × 6 coupons per sample), distributed as follows: 54 non-degassed

FIG. 1 Photographs of the transportation ladle (a), and the FOSECO degassing unit (b) used in the process.

FIG. 2 Symmetric division of a sample to later extract six coupons. On the right side, coupons encapsulated in resin to be polished can be seen.

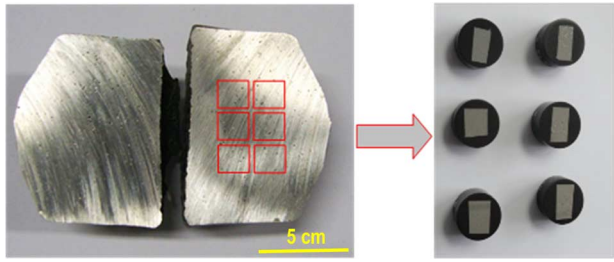

coupons, 18 coupons degassed for 1 min (D (1)), 18 coupons degassed 2 min (D (2)), and 18 coupons degassed for 3 min (D (3)). Notice that the total number of degassed coupons is 54 (18×3), which is in agreement with the one-to-one correspondence between non-degassed and degassed coupons mentioned above. **Table 1** summarizes the experimental scope, including the codes used to identify the samples (the number in parentheses represents the degassing time) as well as the correspondence between non-degassed and degassed samples.

MATERIAL FILTERED AND FILTERED AND DEGASSED

The analysis of the effectiveness of the combination of the filtering and degassing processes was performed using a SIVEX S alumina-based filter with a pore size of 20 ppi and dimensions $508 \times 508 \times 50$ mm^3; following the recommendations for use, it was pre-heated to 700°C–800°C before using it. First, the material was poured from the reverberatory furnace to a Krown filtering furnace where the above-mentioned alumina filter had been previously set up. **Fig. 3** includes two photographs where the pouring and filtering processes (**Fig. 3a**) and the subsequent exit of the filtered material to the transportation ladle (**Fig. 3b**) can be seen. Then the material was degassed in the ladle, employing again a flow rate of 15 L/min; the degassing time in all cases was 1.5 min.

This manufacturing process has allowed three types of samples to be analyzed: (1) non-treated samples, that is, without degassing and without filtration (NDF), (2) filtered samples (F), and (3) filtered and then degassed (1.5 min) samples (FD). The samples of the NDF family were taken directly from the reverberatory furnace; those of the group F were obtained from the ladle before degassing, and, finally, samples belonging to the FD group were taken from the ladle after degassing. The experimental scope includes five castings from which the 15 samples listed in **Table 2** were taken. As can be seen, each of the groups (NDF, F, and FD) include five samples, corresponding to the five castings. It is worth noting too, that these five castings were processed sequentially, stating with Casting #1 to finish with #5. Subsequently, 12 coupons were machined from each one of the samples to conform a total of 180 coupons.

Finally, the temperature of the molten material was determined in the reverberatory furnace and in the transfer ladle (for degassed material, before and after degassing) with the RAYTEC infrared sensor previously mentioned.

The protocol for sample preparation and analysis carried out on these coupons is similar to that previously employed with degassed samples (see above). However, in this case, a microstructural study analyzing the phase distribution was added. Moreover, after completing the sampling, the SIVEX filter was retrieved to be chemically characterized by means of the EDS analyzer equipped in the scanning electron microscopy (SEM).

TABLE 1 Identification codes of the samples as a function of the degassing time.

Non-Degassed	Degassed
ND_1, ND_2, ND_3	D(1)_1, D(1)_2, D(1)_3
ND_4, ND_5, ND_6	D(2)_3, D(2)_4, D(2)_5
ND_7, ND_8, ND_9	D(3)_6, D(3)_7, D(3)_8

Note: The number in parentheses is the degassing time and the final figure is the number of the sample. ND: non-degassed; D: degassed.

Experimental Results and Discussion

RESULTS OF DEGASSING

Analysis of Porosity

Fig. 4a allows the results of porosity obtained in each of the nine non-degassed samples to be compared against the corresponding degassed samples. To facilitate the analysis, the data were presented separately as a function of degassing time (notice that each of the bars in the figure represent the average porosity of six coupons); **Fig. 4b** provides, under the same format, the results of the maximum pore size in each of the samples. Regarding porosity (**Fig. 4**), the results demonstrate the systematic effectiveness of

FIG. 3

Photographs showing the filter process (a), and the subsequent pouring in the ladle for degassing (b).

TABLE 2 Castings and samples available for the filtering and degassing analysis.

Casting #	Samples
1	NDF_1, F_1, FD_1
2	NDF_2, F_2, FD_2
3	NDF_3, F_3, FD_3
4	NDF_4, F_4, FD_4
5	NDF_5, F_5, FD_5

Note: The final figure is the number of the casting. NDF: non-degassed and non-filtered; F: filtered; FD: filtered and degassed.

degassing because, in all cases, the treatment leads to a significant reduction in this parameter. On the other hand, the individual values of maximum pore exhibit a more erratic behavior (see **Fig. 4b**), as in some cases only a slight decrease occurs. This may be regarded as a consequence of the nature of the sampling conducted. In effect, the result of degassing expressed in terms of the maximum pore present is, to some extent, a random phenomenon that strongly depends on the particular location of the small sample selected. Nevertheless, in all cases, the maximum pore size decreases after degassing.

To reach a more realistic description, in **Fig. 5**, the average values of the results are shown, respectively, in **Fig. 4a** and **4b**. The mean values for each time of degassing and the corresponding standard deviations can be appreciated. This presentation helps to eliminate deviations because of the random nature of sampling, particularly evident in the case of the maximum pore size (**Fig. 4b**). Under this form, it can be seen that the degassing technique is effective not only from the perspective of porosity reduction (**Fig. 5a**), but also considering the maximum pore size (**Fig. 5b**). It is worth noting that in this latter case non-negligible values for the standard deviation were obtained.

Another aspect worth analyzing is the relationship between the time of degassing and the improvement in material properties. This is represented in **Fig. 6a** and **6b** for the porosity and the maximum pore size, respectively. Individual values (as red circles) and mean values (blue squares) with their standard deviation are included in the figures. The linear fit of the individual data was added to reveal the average trend in each case. The analysis of **Fig. 6a** is straightforward: a reliable linear relationship between the time of degassing and the reduction in the average values of porosity is observed. According to the slope of the linear fitting carried out, every minute of degassing represents, roughly, a 19 % reduction in porosity. **Fig. 6b** offers a similar behavior showing that a longer degassing time corresponds to a further reduction in the maximum pore size; in this case, each minute reduces the maximum pore by 21 %.

Temperature Loss During Degassing

A final point that has been studied in connection with degassing is that of the temperature loss in the molten material. This is of great importance in the field of HPDC because the molten material must reach the injector with a temperature high enough so that its viscosity is sufficiently small to allow the proper filling of the mold. On the contrary, when the temperature of the material becomes too high, several problems arise. Thus, the aluminum reacts with oxygen in the atmosphere and generates precipitates of Al_2O_3, which compromise the final quality of the molded part. In addition, the solubility of hydrogen increases exponentially with temperature; roughly, an increase of ~100°C doubles this solubility [3]. All things being equal, a higher temperature of an aluminum melt will increase the necessary degassing time. Consequently, it is essential to evaluate the temperature loss during the degassing to avoid falling into one of these two pernicious scenarios.

Three temperatures were recorded during the process: first, the temperature of the molten material in the reverberatory furnace (T1); second, the temperature of the material in the transfer ladle after being poured from the furnace (T2); and, finally, the temperature in the ladle after degassing (T3). All these values are collected in **Table 3** where the significant differences T1-T2 and T2-T3 are also included.

FIG. 4 Average porosity (a), and area of the maximum pore (b) obtained in each of the samples before and after degassing.

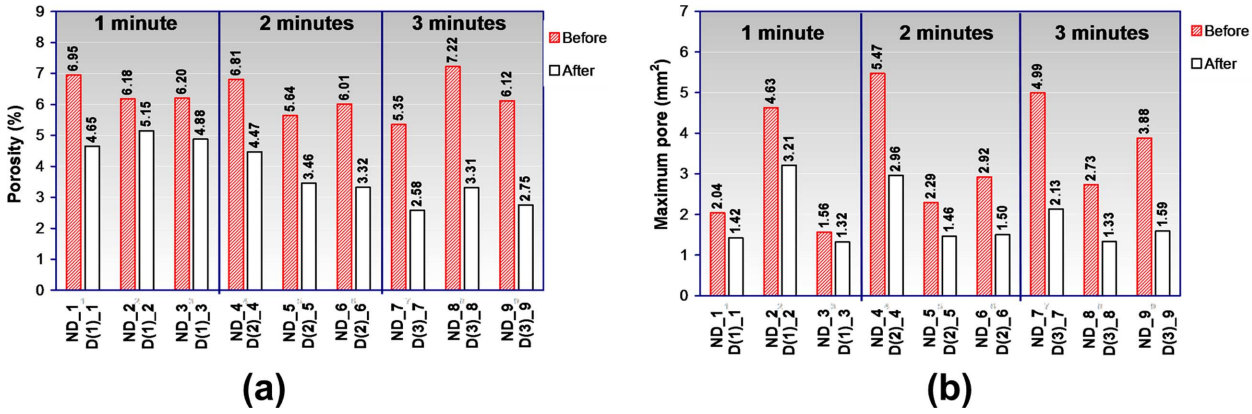

FIG. 5 Average porosity (a), and average area maximum pore (b) depending on the time of degassing.

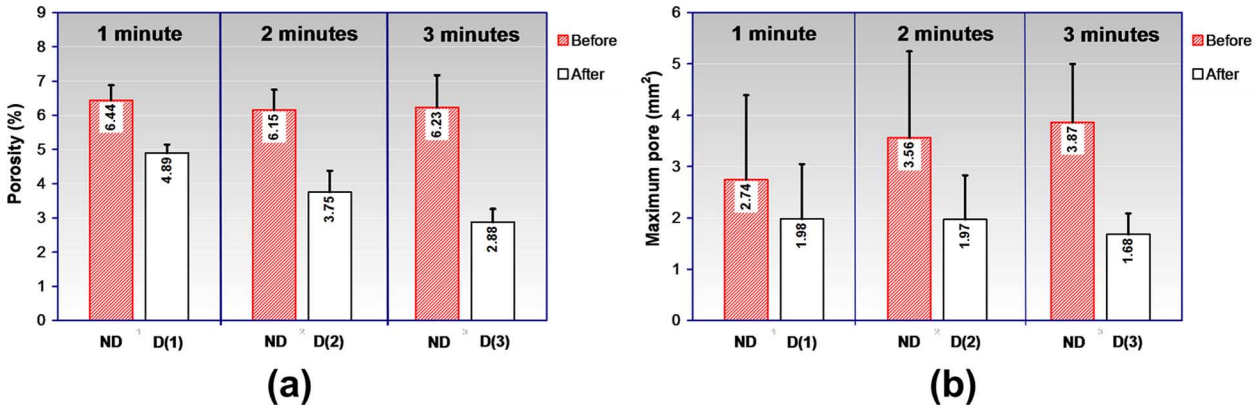

FIG. 6

Representation of the decrease in porosity (a), and in maximum pore size (b) as a function of the time of degassing.

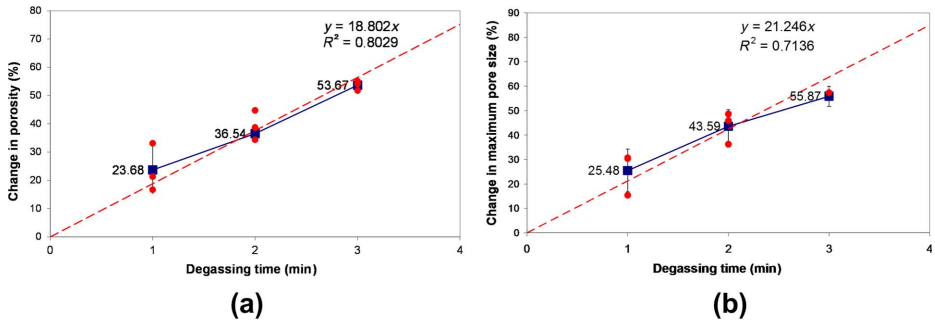

TABLE 3 Relevant results concerning the temperature loss during degassing.

Sample	T1 (°C)	T2 (°C)	T3 (°C)	T1-T2	T2-T3
D(1)_1	895	855	805	40	50
D(1)_2	865	820	785	45	35
D(1)_3	885	850	790	35	60
D(2)_1	875	825	745	50	80
D(2)_2	880	855	780	25	75
D(2)_3	900	860	775	40	85
D(3)_1	870	835	745	35	90
D(3)_2	870	840	745	30	95
D(3)_3	875	825	740	50	85

Note: T1 is the temperature of the molten material in the reverberatory furnace, T2 is the temperature of the material in the ladle after being poured from the furnace, and T3 is the temperature in the ladle after degassing.

Fig. 7 allows the relationship between the time of degassing and temperature loss T2-T3 (that is to say, the temperature loss because of degassing) in the material to be appreciated. A clear upward trend in the results can be observed. The average temperature losses are 48°C ± 13°C for 1 min, 80°C ± 5°C for 2 min, and 90°C ± 5°C for 3 min. At first sight, these absolute values of temperature loss may seem high. They depend, in the first place, on the characteristics of the insulation system used in the transportation ladle where the degassing was carried out (see details above). Moreover, it is worth mentioning that the transportation ladle was feeding only one HPDC injection machine and, as a result, it was working discontinuously. Consequently, the time between two successive ladle fillings allowed some temperature to be lost, thus affecting the temperature of the molten aluminum of the following degassing operation. In any case, as mentioned above, the aim here is to reproduce the actual operating conditions in the plant.

The figure includes a linear fit of the data according to which every minute of degassing means, roughly, a temperature loss of 34°C. However, to improve the quality of the fitting, a logarithmic expression was used as well. This has the advantage of naturally reproducing the phenomenon of attenuation in the temperature loss that occurs as the time of degassing increases. Therefore, as can be seen, it fits the values in the figure in a more reliable way. Besides, the maximum difference between the average values of temperature loss and the predictions of the model is less than 5.0 %.

RESULTS OF FILTRATION AND DEGASSING

Analysis of Porosity

Fig. 8 shows an analysis of the influence of filtration and the combination of this process with degassing on the porosity. Data are

FIG. 7 Temperature loss during degassing as a function of degassing time.

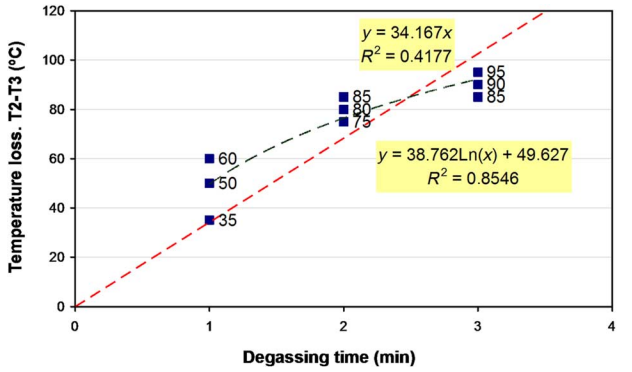

organized by casting (Castings #1 to #5, see **Table 2**) and group (NDF, F, and FD), including the average value and the standard deviation. Even taking into consideration the statistical dispersion, it is possible to draw well-established conclusions. Thus, for Castings #2, #3, and #4, the results show clearly that filtering collaborates in reducing the porosity of the samples; this feature is also present in the case of Castings #1 and #5, but is less marked. The influence of degassing, in turn, can be seen by observing that in all cases this process leads to a systematic reduction in porosity with respect to the filtered samples. Considering the average values, filtering reduces the porosity by 10 %, whereas degassing additionally collaborates by 28 %; this last result is perfectly consistent with the values previously offered in **Fig. 6a**.

The study carried out regarding the maximum pore size is summarized with a similar format in **Fig. 9**. The conclusions previously drawn concerning the porosity may be transferred point by point to this case. Thus, filtering reduces this parameter by 21 %, whereas degassing additionally collaborates by 26 %. Again, this last result is consistent with the values set forth above in **Fig. 6b**.

Analysis of the Effectiveness of Filtration to Remove Inclusions

$AlSi_9Cu_3$ alloy in the as-cast condition shows a microstructure that includes various phases. According to the literature [23–26], alpha phase (α), eutectic silicon, and many intermetallic phases, such as Fe- and Cu-rich phases with different morphology can be distinguished. **Fig. 10a** shows an optical micrograph that allows the typical distribution of phases in the material to be appreciated: the aluminum-rich phase α (a), an eutectic region (b), mixture of α-matrix and Si-needles and various intermetallic compounds (c and d) can be seen. The chemical nature of the various phases was determined using the EDS microanalysis device of the SEM microscope (Carl Zeiss EVO MA15 model). Results are shown in **Fig. 10b1–10d2**. In **Fig. 10b1** and **10b2**, the chemical composition of the α-region is analyzed; the results make it possible to verify that this phase is composed exclusively of aluminum. The analysis shown in **Fig. 10c1** and **10c2** presumably corresponding to the common iron intermetallic $Al_{15}(MnFe)_3Si_2$, which has a compact morphology in the form of "Chinese script" or "skeleton-like" [12]. Finally, the location chemically characterized in **Fig. 10d1** and **10d2** corresponds to an eutectic Si-rich region.

One of the aims of this study is to determine the efficiency of filtering and degassing processes to remove inclusions, intermetallic phases, etc. A first alternative to undertake this task would be to quantify and to compare the amount of inclusions present in non-treated samples, filtered and filtered and degassed samples, respectively. This direct method, however, seems to be extremely

FIG. 8
Average porosity and standard deviation obtained from each casting [1–5] and group (NDF, F, FD).

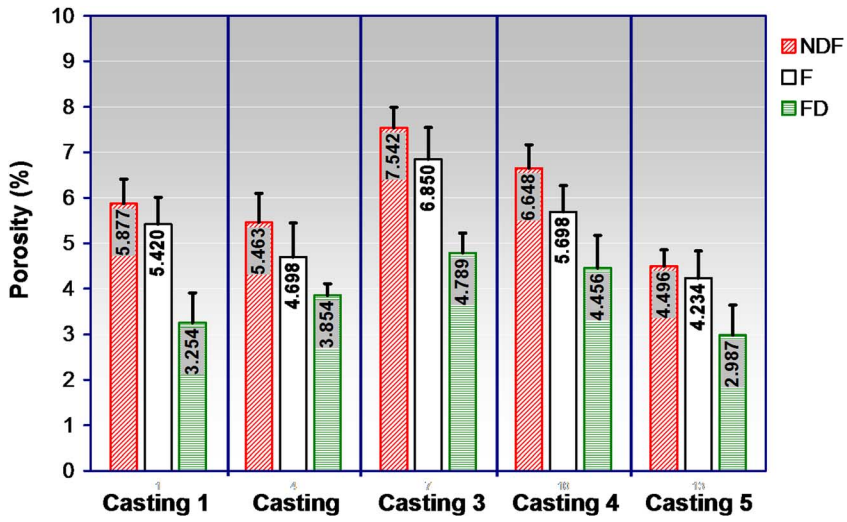

FIG. 9

Average maximum pore size and standard deviation obtained from each casting [1–5] and group (NDF, F, FD).

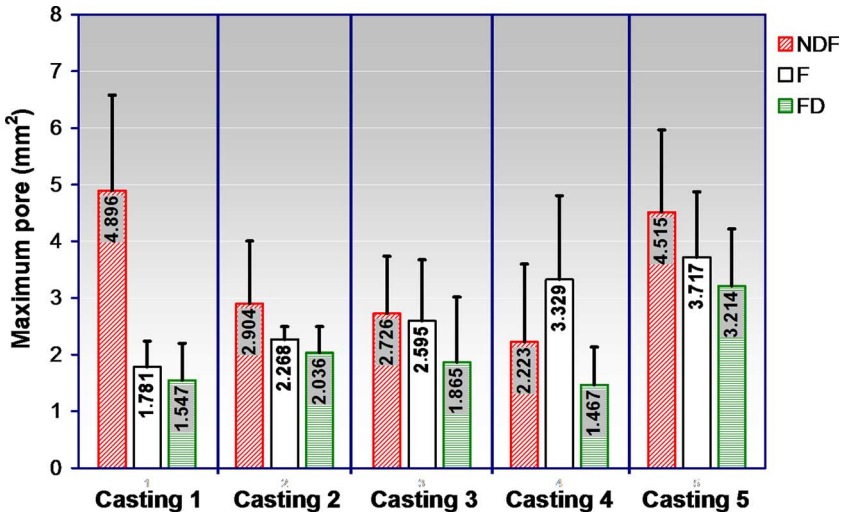

laborious and probably doomed to failure unless an enormous experimental work including a large number of samples is conducted. For this reason, in this research, an indirect alternative methodology was used consisting in quantifying the presence of α-phase in the samples of the three groups studied: NDF, F, and FD. The logic of this procedure lies in the fact that an increase in the amount of α-phase after treating the material through filtering or degassing must correspond to a reduction in inclusions and intermetallic phases; in other words, it is an indirect method to assess the effectiveness of the treatments of filtration and degassing to remove undesired elements in the material. To determine the amount of α-phase, all samples were scanned by optical microscopy and further analyzed with Olympus analysisFIVE software capable of automatically quantifying the presence of that phase.

Fig. 11 allows the results to be appreciated. As can be seen, the filtered material significantly increases the presence of α-phase (or, in other words, decreases by the same amount the number of undesirable particles). Moreover, the joint action of the filtering and degassing processes slightly improves the previous result; nevertheless, this should be viewed with caution in consideration of the values obtained for the standard deviation (also represented in the figure).

To confirm the coherence of the results, a study of the chemical composition of the particles located in the filter used for cleaning the samples was conducted. In this sense, a set of fragments taken from the filter used to clean the molten material were chemically characterized by EDS to determine the chemical composition of the particles retained therein. The scope of this analysis was limited to the chemical characterization of several tens of particles; in spite of not being an exhaustive study, this made it possible to confirm that the particles retained in the filter are in the form of oxides with presence of elements like Al, Si, Mn, Ca, and Fe. Such particles fit very well with the different phases identified by the optical and SEM microscopy previously shown in **Fig. 10**.

Temperature Loss During Filtering and Degassing

In this section, the results of temperature loss as a result of filtering and degassing are presented. Therefore, it complements the information provided previously where only the consequences of the degassing were studied. Three temperatures were recorded during the process: (1) the temperature of the molten material in the reverberatory furnace (T1), (2) the temperature of the material after being filtered (T2), and, finally, (3) the temperature in the ladle after filtering and degassing (T3). The results obtained are gathered in **Table 4**. The first aspect that draws attention is that the reduction in the material temperature because of filtering is substantially higher than that produced by the subsequent degassing. Thus, the average value of T1-T2 is 170°C ± 12°C, whereas for T2-T3 it is 39°C ± 7°C. This result is slightly smaller to what is expected in view of the information represented in **Fig. 7**; nevertheless, it must be taken into account that in this case the initial temperature in the degassing process is noticeably smaller because of the previous action of filtration.

Temperature is one of the most common limiting factors in HPDC because the minimum temperature of the molten material during injection must be ~640°C; otherwise, the high viscosity may lead to partial fillings, especially for complex shapes. As mentioned above, Castings #1 to #5 were processed sequentially; as can be seen in **Table 4**, as the number of casting increases, the temperature loss decreases. This is because of the heating that the filtering system is undergoing (even though it was pre-heated before starting the process). In some cases, the thermal inertia of the filter is so high that a number of castings must be "sacrificed" before reaching the steady-state condition (the first castings are just used to adjust the temperature of the transportation ladle,

FIG. 10

Illustrative results of the microstructural analysis carried out by SEM and EDS microanalysis.

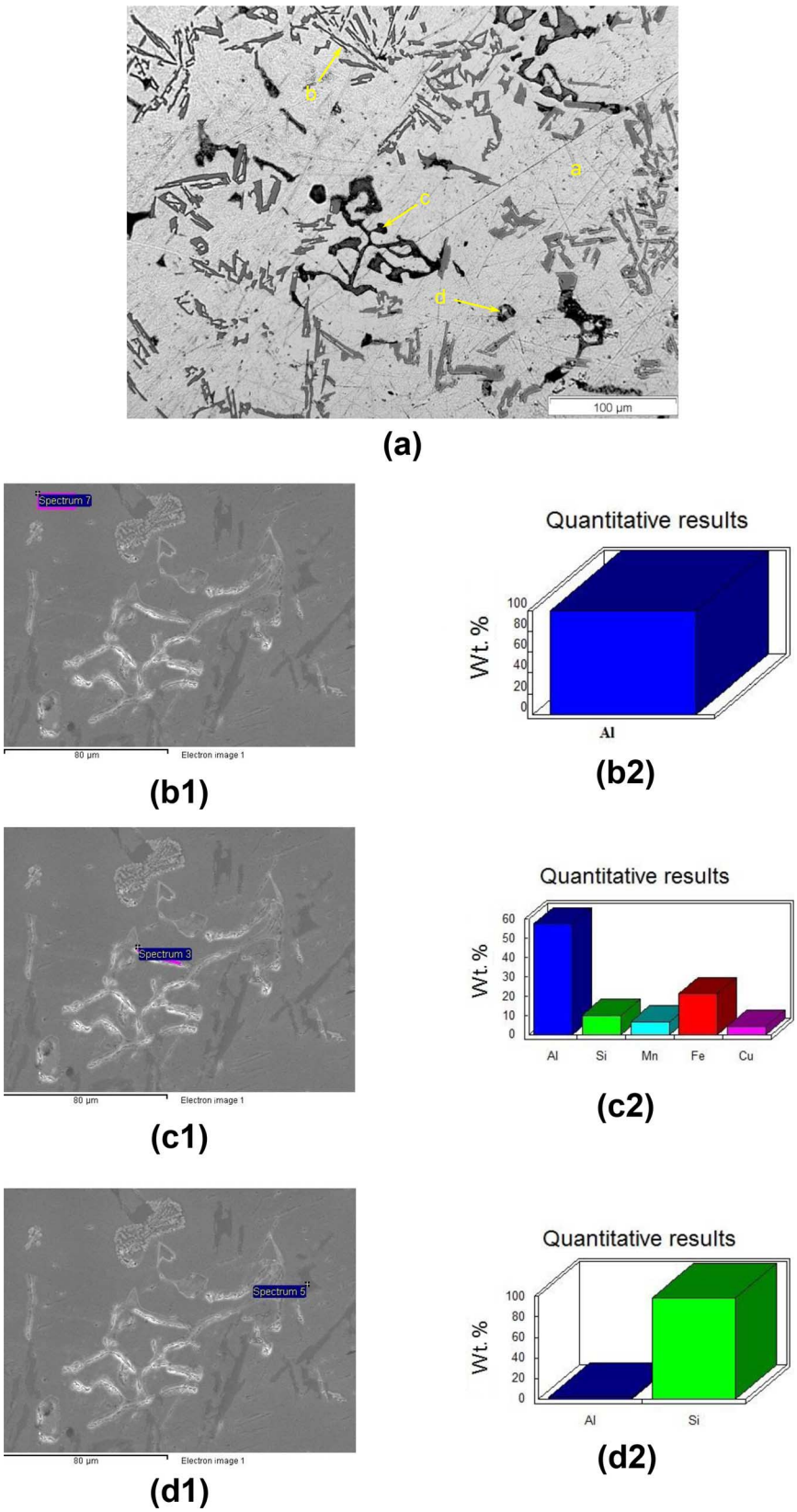

FIG. 11 Presence of α-phase in untreated (NDF), filtered (F), and filtered and degassed (FD) samples.

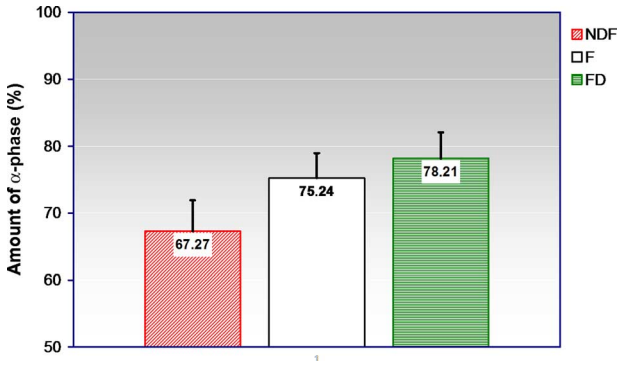

TABLE 4 Relevant results concerning the temperature loss during filtering and degassing.

Casting #	T1 (°C)	T2 (°C)	T3 (°C)	T1-T2	T2-T3	T1-T3
1	860	670	630	190	40	230
2	865	695	650	170	45	215
3	880	710	665	170	45	215
4	890	730	700	160	30	190
5	870	710	675	160	35	195

Note: T1 is the temperature of the molten material in the reverberatory furnace, T2 is the temperature of the material after being filtered, and T3 is the temperature in the ladle after filtering and degassing.

filters, etc.). For instance, in this research, Castings #1, #2, and #3 were rejected (they were re-introduced into the reverberatory furnace, which is a common practice in foundries).

Summary and Conclusions

The present experimental work has allowed the determination of the influence of the filtering and degassing procedures on the properties of the $AlSi_9Cu_3$ alloy. Specifically, the porosity of the material and the amount of inclusions present in untreated samples and in degassed and filtered samples were measured. Furthermore, the thermal loss that occurs as a consequence of the application of each of these treatments was evaluated. The manufacture of the samples was carried out in an industrial facility currently in service dedicated to the manufacturing of components in alloy $AlSi_9Cu_3$. The studies concerning the material properties have been developed in the laboratory LADICIM of the University of Cantabria (Cantabria, Spain).

The degassing of the material was carried out by bubbling nitrogen at a flow rate of 15 L/min. Regarding this treatment, the work has allowed the following conclusions to be reached:

- The aggregate analysis of the experimental results shows that both the porosity of the material and the maximum pore size are reduced after the degassing. It has also been observed that the efficiency of the treatment in terms of the porosity is improved by increasing the time of degassing. Thus, according to the linear fit carried out, every minute of degassing represents an approximate 19 % and 21 % reduction in porosity and maximum pore size, respectively.
- With regard to the loss of temperature, the following values have been recorded: 48°C ± 13°C for 1 min, 80°C ± 5°C for 2 min, and 90°C ± 5°C for 3 min. The data were fitted through a linear relation according to which every minute of degassing means, roughly, a temperature loss of 34°C. Nevertheless, better results were achieved by using a logarithmic expression: in this case, the maximum difference between the average values of temperature loss and the predictions of the expression is less than 5.0 %.

The analysis of filtration was conducted using a 20-ppi alumina-based filter. Three types of samples were characterized: (1) non-treated samples, (2) filtered samples, and (3) filtered and then degassed (1.5 min). The following conclusions can be enumerated:

- Filtering and degassing both contribute to reducing the porosity of the molten material. Thus, filtering reduces the porosity by 10 %, whereas degassing additionally collaborates by 28 %. In the same way, filtering reduces the maximum pore size by 21 %, whereas degassing additionally collaborates by 26 %.
- Regarding the presence of inclusions, the experimental results demonstrate that filtration improves the quality of the material. Moreover, the joint action of the filtering and degassing processes slightly improves this result.
- The above two findings support the conclusion that both processes act synergistically: filtering works together with degassing to reduce porosity and, simultaneously, degassing works together with filtration to remove inclusions. Therefore, it is recommended to combine filtration and degassing to achieve an optimal final quality of the material.
- Regarding the loss of temperature, the influence of filtering is substantially higher than that produced by the subsequent degassing (170°C ± 12°C for filtration compared to 39°C ± 7°C for degassing).
- SEM-EDS microanalysis allowed the inclusions retained in the filter to be located and their chemical composition to be determined. It was demonstrated that their chemical composition corresponds to that of the inclusions previously found in non-treated samples. In this manner, it was possible to verify the similarity between the nature of the particles retained by the filter and the inclusions present in the untreated material.

ACKNOWLEDGMENTS

This investigation was developed within a research project sponsored by the Society for the Regional Development of Cantabria (SODERCAN). The writers express particular gratitude to their

colleagues Eng. Lorenzo Gutiérrez Malde and Eng. Rafael Fernández Iglesias for their contribution to the experimental work and analysis of results.

References

[1] Akhtar, S., Dispinar, D., and Arnberg, L., "Effect of Hydrogen Content, Melt Cleanliness and Solidification Conditions on Tensile Properties of A356 Alloy," *Int. J. Cast Metals Res.*, Vol. 22, Nos. 1–4, 2009, pp. 22–25.

[2] Sigworth, G. K., *Best Practices in Aluminum Metalcasting*, American Foundry Society, Schaumburg, IL, 2014, 296 pp.

[3] American Society for Metals, *Metals Handbook: Casting*, Vol. 15, 9th ed., ASM International, Materials Park, OH, 1988.

[4] Ignaszak, Z. and Hajkowski, J., "Contribution to the Identification of Porosity Type in AlSiCu High-Pressure-Die-Castings by Experimental and Virtual Way," *Arch. Foundry Eng.*, Vol. 15, No. 1, 2015, pp. 143–151.

[5] Samuel, A. and Samuel, F., "Effect of Melt Treatment, Solidification Conditions and Porosity Level on the Tensile Properties of 319.2 Endchill Aluminium Castings," *J. Mater. Sci.*, Vol. 30, No. 19, 1995, pp. 4823–4833, https://doi.org/10.1007/BF01154490

[6] Radhakrishnan, K., Seshan, S., and Seshadri, M., "Effect of Porosity on Mechanical Properties of Aluminum-Alloy Castings," *Trans. Indian Inst. Metals*, Vol. 34, No. 2, 1981, pp. 169–171.

[7] Samuel, A. and Samuel, F., "A Metallographic Study of Porosity and Fracture Behavior in Relation to the Tensile Properties in 319.2 End Chill Castings," *Metall. Mater. Trans. A*, Vol. 26, No. 9, 1995, pp. 2359–2372, https://doi.org/10.1007/BF02671250

[8] Surappa, M., Blank, E., and Jaquet, J., "Effect of Macro-Porosity on the Strength and Ductility of Cast Al-7Si–0.3Mg Alloy," *Scripta Metall.*, Vol. 20, No. 9, 1986, pp. 1281–1286, https://doi.org/10.1016/0036-9748(86)90049-9

[9] Cáceres, C., "On the Effect of Macroporosity on the Tensile Properties of the Al-7 %Si-0.4 %Mg Casting Alloy," *Scripta Metall. Mater.*, Vol. 32, No. 11, 1995, pp. 1851–1856, https://doi.org/10.1016/0956-716X(95)00031-P

[10] Ignaszak, Z., Popielarski, P., and Hajkowski, J., "Problem of Acceptability of Internal Porosity in Semi-Finished Cast Product as New Trend 'Tolerance of Damage' Present in Modern Design Office," *Defect Diffus. Forum*, Vols. 326–328, No. 1, 2012, pp. 612–619.

[11] Badanoiu, A., 2005, "High Porosity on Ceramic Materials," *Scientific Journal of Scientometry*, Vol. 17, No. 1, pp. 1–19.

[12] Birol, Y., "Survey of Inclusions in Twin Roll Casting of Wrought Aluminium Alloys," *Int. J. Cast Metals Res.*, Vol. 23, No. 4, 2010, pp. 250–255, https://doi.org/10.1179/136404610X12693537269930

[13] Cao, X., "Calculation of Solid Inclusion Concentrations from Filter Cakes," *Int. J. Cast Metals Res.*, Vol. 19, No. 6, 2006, pp. 371–374, https://doi.org/10.1179/136404606X169914

[14] Cui, J. and Roven, H. J., "Recycling of Automotive Aluminum," *Trans. Nonferr. Metals Soc. China*, Vol. 20, No. 11, 2010, pp. 2057–2063, https://doi.org/10.1016/S1003-6326(09)60417-9

[15] Dispinar, D., Akhtar, S., and Nordmark, A., "Degassing, Hydrogen and Porosity Phenomena in A356," *Mater. Sci. Eng. A*, Vol. 527, Nos. 16–17, 2010, pp. 3719–3725, https://doi.org/10.1016/j.msea.2010.01.088

[16] Hurtalova, L., Belan, J., and Tillova, E., "Changes in Structural Characteristics of Hypoeutectic Al-Si Cast Alloy After Age Hardening," *Mater. Sci.*, Vol. 18, No. 3, 2012, pp. 228–233.

[17] Ogris, E., Wahlen, A., and Lüchinger, H., "On the Silicon Spheroidization in Al-Si Alloys," *J. Light Met.*, Vol. 2, No. 4, 2002, pp. 263–269, https://doi.org/10.1016/S1471-5317(03)00010-5

[18] Carcea, I. and Gherghe, M., Nonferrous Foundry, *Gheorghe Asachi*, Technical University of Iași, Iași, Romania, 2012.

[19] Olson, R. A. and Martins, L. C., "Cellular Ceramics in Metal Filtration," *Adv. Eng. Mater.*, Vol. 7, No. 4, 2005, pp. 187–192, https://doi.org/10.1002/adem.200500021

[20] Moldovan, P., Panait, N., and Marginean, S., *Fundamentals of Melting of Nonferrous Metals*, Intact, Bucharest, Romania, 1998.

[21] Panušková, M., Tillová, E., and Chalupová, M., 2008, "Relation Between Mechanical Properties and Microstructure of Cast Aluminum Alloy $AlSi_9Cu_3$," *Strength Mater.*, Vol. 40, No. 1, 2005, pp. 98–101.

[22] Pucher, P., Bottcherz, H., and Kaufmanns, H., "$AlSi_9Cu_3$ (Fe)(A226)," *TMS 2011 140th Annual Meeting and Exhibition, Materials Fabrication, Properties, Characterization, and Modeling*, Vol. 2, San Diego, CA, Feb. 27–March 3, 2011, The Minerals, Metals and Materials Society, Pittsburgh, PA, 2011, 237 pp.

[23] Puga, H., Barbosa, J., and Seabra, E., "New Trends in Aluminium Degassing—A Comparative Study," presented at the *Fourth International Conference on Advances and Trends in Engineering Materials and Their Applications, AES-ATEMA*, Hamburg, Germany, Sep. 1–4, 2009, Advanced Engineering Solutions, Ottawa, ON, Canada.

[24] Shih, T., Huang, L., and Chen, Y., "Relative Porosity in Aluminium and in Aluminium Alloys," *Int. J. Cast Metals Res.*, Vol. 18, No. 5, 2005, pp. 301–308, https://doi.org/10.1179/136404605225023135

[25] Tillová, E., Chalupová, M., and Hurtalová, L., "Structural Analysis of Heat Treated Automotive Cast Alloy," *J. Achieve. Mater. Manuf. Eng.*, Vol. 47, No. 1, 2011, pp. 19–25.

[26] Uemura, K., Takahashi, M., and Koyama, S., "Filtration Mechanism of Non-Metallic Inclusions in Steel by Ceramic Loop Filter," *ISIJ Int.*, Vol. 32, No. 1, 1992, pp. 150–156.